Chemical Engineering Journal 511 (2025) 161918

Contents lists available at ScienceDirect

Chemical Engineering Journal

journal homepage: www.elsevier.com/locate/cej

Selective conversion of aqueous sorbitol to sorbitan by amorphous Silica-Alumina catalysts

Napat Lertthanaphol [a], Pakawan Sereerattanakorn [a,b], Sarttrawut Tulaphol [c], Thana Maihom [d], Thanh Khoa Phung [a,e], Gabriella Garbarino [f,g], Guido Busca [f,g], Jatuporn Wittayakun [b], Vance Jaeger [a], Shashi B. Lalvani [h], Noppadon Sathitsuksanoh [a,*]

[a] Department of Chemical Engineering, University of Louisville, Louisville, KY 40292, USA
[b] School of Chemistry, Institute of Science, Suranaree University of Technology, Nakhon Ratchasima 30000, Thailand
[c] Sustainable Polymer & Innovative Composite Materials Research Group, Department of Chemistry, Faculty of Science, King Mongkut's University of Technology Thonburi, Bangkok 10140, Thailand
[d] Department of Chemistry, Kasetsart University, Kamphaeng Saen Campus, Nakhon Pathom 73140, Thailand
[e] School of Chemical and Environmental Engineering, International University, Vietnam National University – HCMC, Ho Chi Minh City, Vietnam
[f] Department of Civil, Chemical and Environmental Engineering, Chemical Engineering pole, University of Genova, via Opera Pia 15, 16146 Genova, Italy
[g] INSTM udr di Genova, via Dodecaneso 31, 16146 Genova, Italy
[h] Department of Chemical, Paper, and Biomedical Engineering, Miami University, Oxford, OH 45056, USA

ARTICLE INFO

Keywords:
Aqueous sorbitol
Dehydration
Sorbitan
Amorphous silica-alumina
Isosorbide

ABSTRACT

Biomass-derived chemicals are key enablers of a circular bioeconomy, offering renewable solutions to mitigate climate change. Notably, 1,4-sorbitan is a versatile platform chemical for food, chemical, and pharmaceutical industries. We can obtain 1,4-sorbitan from solid acid-catalyzed dehydration of biomass-derived sorbitol. However, the instability and poor selectivity of most solid acid catalysts in aqueous sorbitol significantly hinder the efficient production of 1,4-sorbitan, limiting their industrial viability. Here, we show that the hydrothermal stability and optimal Brønsted acid strength of commercial amorphous silica-alumina with 40 wt% silica enabled high selectivity of 1,4-sorbitan (65 %) derived from aqueous sorbitol. The silica in amorphous silica-alumina catalysts provided optimal Brønsted acidity that minimized the degradation of the desired 1,4-sorbitan product by preventing further dehydration to isosorbide and polymerization to coke. Moreover, the silica content in amorphous silica-alumina catalysts improved the hydrothermal stability and prevented the phase transformation of the γ-alumina matrix. Our findings demonstrate that amorphous silica-alumina is a highly selective catalyst for 1,4-sorbitan production from aqueous sorbitol, and amorphous silica-alumina offers enhanced stability. These findings pave the way for designing improved solid acid catalysts for other sustainable, aqueous biomass conversions.

1. Introduction

Producing biofuels and biochemicals from renewable biomass feedstocks is a promising route toward net-zero emissions and circular bioeconomy. The compound 1,4-sorbitan is a platform chemical for surfactants that can be used as emulsifiers, insecticides, food additives, pharmaceuticals, preservatives in personal care products and components in drug delivery systems [1–4]. For example, sorbitan caprylate is used as a preservative for cosmetics. Sorbitan monolaurates can be used as animal feed [5]. Sorbitan stearate and palmitate can be used as drug carriers [6]. To produce 1,4-sorbitan, biomass-derived glucose is hydrogenated to sorbitol (Fig. 1), and the sorbitol is dehydrated by acid catalysts to create 1,4-sorbitan [7]. Homogenous acid catalysts such as H_2SO_4 are used in industrial production of 1,4-sorbitan [8]. For example, Yabushita et al. [9] used sulfuric acid with neat sorbitol (water-free) at 130 °C and obtained a high 1,4-sorbitan selectivity of 63 %. Dabbawala et al. [10] investigated various homogeneous acid catalysts, including sulfuric acid, triflic acid, and boric acid, with neat sorbitol at 160–180 °C. They found that boric acid at 180 °C for 1 h gave the highest sorbitans selectivity of 90 % with 41 % conversion.

* Corresponding author.
E-mail address: n.sathitsuksanoh@louisville.edu (N. Sathitsuksanoh).

https://doi.org/10.1016/j.cej.2025.161918
Received 17 October 2024; Received in revised form 28 February 2025; Accepted 23 March 2025
Available online 24 March 2025

Nevertheless, although they are selective, homogeneous acids are corrosive, they create hazardous wastes, and they complicate product separation, all contributing to the production cost of 1,4-sorbitan [9,11]. Consequently, investigators are focused on developing active and selective solid acid catalysts for conversion of aqueous sorbitol.

Various types of solid heterogenous acid catalysts, such as zeolites [12–15], metal oxides [16], and acid resins [17–21], are effective for aqueous sorbitol dehydration. However, these acid catalysts are often associated with low 1,4-sorbitan selectivity because of continuous dehydration and catalyst deactivation. For example, Boupan et al. [18] used acid resins, Purolite CT269, and obtained a high 1,4-sorbitan selectivity of ~58 % at 74 % conversion of aqueous sorbitol. However, this catalyst deactivated quickly. Bonnin et al. [4] showed 67 % selectivity to combined 1,4- and 3,6-sorbitans at ~100 % conversion of aqueous sorbitol using 30 bar CO_2. Although effective, the high-pressure operation could increase the capital and operational costs of 1,4-sorbitan production. Moreover, water molecules produced by the dehydration reaction and from the medium can competitively adsorb on active sites, altering acid properties, causing catalyst deactivation, and producing undesired by-products (e.g., humin) [17,19,22]. Otomo et al. [15] reported that Hβ(75) zeolites (Si/Al molar ratio of 75) catalyzed aqueous sorbitol and yielded ~47 % 1,4-sorbitan with ~90 % conversion at 180 °C for 12 h. After one use, the catalyst was deactivated and showed 28 % decrease in catalytic activity. Likewise, Zhang et al. [23] dehydrated aqueous sorbitol with sulfated zirconia catalysts at 140–220 °C and found catalyst deactivation due to sulfur loss. Therefore, we need to develop more stable and selective solid acid catalysts for sorbitol dehydration [14].

Amorphous silica-alumina catalysts (ASA) are unique solid acid catalysts that have stronger acidity than γ-alumina but weaker acidity than zeolites [24]. Similar to zeolites, the silica in the alumina matrix of ASA provides both Brønsted acid sites (BAS) and Lewis acid sites (LAS), but a milder BAS compared with zeolites [25,26]. Moreover, the strengths of Brønsted acid and Lewis acid sites are tunable by tailoring the silica-alumina ratio [27]. In addition, this silica incorporation enhances structural stability against sintering at high temperature (up to 1200 °C) [28]. These characteristics make ASA versatile for biomass conversion reactions [29,30]. Li and Huber [7] dehydrated aqueous sorbitol with ASA catalysts. However, there is no report on the relationship between acid properties and catalytic performance of ASA for aqueous sorbitol conversion. Understanding the relationship between the properties and function of ASA catalysts will guide the design of solid acid catalysts to produce 1,4-sorbitan from aqueous sorbitol.

In this study, we sought to determine the acid properties of ASA and to identify the functions of their active sites responsible for the dehydration of aqueous sorbitol. An ASA with 40 wt% silica (ASA40) showed a high sorbitan selectivity of 65 % at 65 % sorbitol conversion. Importantly, ASA40 was reusable four times with no significant loss of activity or selectivity. This high selectivity and reusability of ASA40 was derived from hydrothermal stability and optimal acid strength. These findings reveal ASA's unrecognized catalytic performance and robustness for selective dehydration of aqueous sorbitol.

2. Materials and methods

2.1. Materials

Amorphous silica-alumina catalysts were obtained from Sasol Germany GmbH (Germany) under commercial names, Siralox® 5/320 (5 wt % silica), 30/270 (30 wt% silica), and 40/270 HPV (40 wt% silica). Before use, the catalysts were pretreated by washing with deionized water to remove impurities, dried at 100 °C for 12 h, and stored in desiccators. All chemicals were used as received unless otherwise noted. Their manufacturers, CAS numbers, and purity are listed in **Table S1.**

2.2. Catalyst characterization

2.2.1. N_2 adsorption–desorption measurement for surface area and pore characteristics

The catalysts' surface areas, pore sizes, and pore volumes were measured by N_2 adsorption–desorption using a Tristar (Micromeritics, USA) instrument. Before the measurement, samples were pretreated at 150 °C for 4 h using a FlowPrep with sample degasser (Micromeritics, USA). The surface area, S_{BET}, was determined from N_2 isotherms by Brunauer–Emmett–Teller equation (BET) at −196.1 °C [31]. BET surface area was calculated over the range of relative pressures between 0.05 and 0.3. The pore volume was estimated from the N_2 desorption values according to the Barrett–Joyner–Halenda (BJH) model [32]. The pore volume was calculated as the uptake (cm^3/g) at a relative pressure of 0.95. We measured the average pore sizes of the samples by the BJH model [33]. The micropore volume was calculated by the t-plot method [34].

2.2.2. Dynamic infrared spectroscopy with pyridine adsorption

The acid densities of the Lewis and Brønsted acid catalysts were measured by the pyridine adsorption method with infrared spectroscopy (IR) [35]. IR spectra were recorded by a Nicolet 380 Fourier-transform Infrared (FTIR) spectrometer (100 scans, 4 cm^{-1} resolution) using the catalyst wafers (~30 mg, area of 1.31 cm^2). The wafers were activated in the customized glass IR cell connected with a conventional outgassing/gas-manipulation apparatus at 500 °C under vacuum (10^{-5} torr) for 1 h. First, the IR spectra of the activated surfaces were collected. Then, the activated samples were contacted with pyridine vapor (P_{Py} ~1 torr) at ambient temperature for 15 min to ensure saturation. Next, the IR spectra of the surface species were collected with and without outgassing at ambient temperature and elevated temperature in the range 50–500 °C with 50 °C increments. On the basis of these recorded spectra, we determined the densities of Lewis(L) and Brønsted(B) acid sites described [36]. In short, the acid density was calculated by the following equation:

$$\text{Acid density } \left(\frac{B}{L}\right) = \varepsilon \left(\frac{B}{L}\right) \text{x } I_A \left(\frac{B}{L}\right) \text{x } \frac{\pi R^2}{W}$$

where ε is the integrated molar extinction coefficients (ε = 1.67 cm/μmol for Brønsted acid sites, and 2.22 cm/μmol for Lewis acid sites), I_A (B, L) the integrated absorbances (cm^{-1}), R the radius of catalyst disk (cm), and W is the weight of disk (mg).

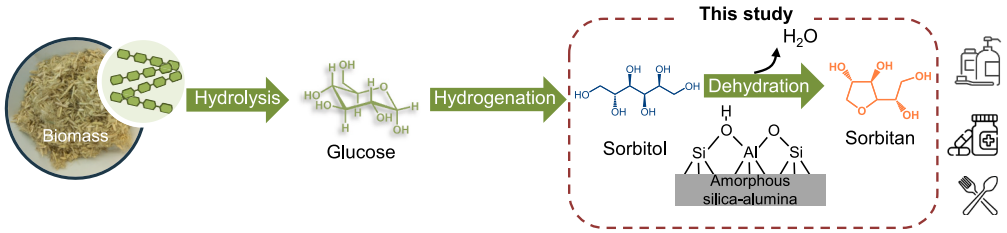

Fig. 1. Schematic illustration of the biomass conversion to sorbitan by amorphous silica-aluminas.

2.2.3. Determination of acid sites by pyridine-diffuse reflectance infrared Fourier transform spectroscopy

Adsorbed pyridine with Diffuse Reflectance Infrared Fourier Transform Spectroscopy (pyridine-DRIFTS) was performed to characterize the acid sites. Temperature-programmed desorption was conducted with the JASCO FTIR (JASCO, USA) equipped with a high-temperature DiffuseIR™ cell (PIKE Technology, WI, USA). The sample treatment and DRIFTS experiments with temperature-programmed desorption were conducted with a slight modification as described [37]. In short, the catalyst sample (~5 mg) was placed in a cylindrical alumina crucible and treated in N_2 gas (50 mL/min) at 130 °C for 60 min unless otherwise noted. After the pretreatment, the sample was cooled to 30 °C. The DRIFT spectrum of the fresh catalyst was recorded as the background spectrum. The samples were then saturated with pyridine vapor by the flow of N_2 gas (50 mL/min). Then, the physisorbed pyridine was removed by flushing it with N_2 gas (50 mL/min) at 220 °C for 30 min before recording the DRIFT spectra. All spectra were recorded with 256 scans between 4000 – 400 cm^{-1} at a 4 cm^{-1} resolution. The basic molecule, pyridine, was protonated by Brønsted acidic OH groups, generating a band at 1540 cm^{-1} and coordinated on Lewis acid sites, resulting in a band at 1450 cm^{-1}.

2.2.4. NH_3-temperature programmed desorption measurement

The catalyst's total acidity was measured by NH_3-temperature programmed desorption (TPD) using the ChemiSorb 2750 with ChemiSoftTPx software (Micromeritics, USA). A quartz U-tube was filled with 0.05 g of fresh catalyst. Prior to testing, all adsorbed water and organic matter were dried by flowing helium through a catalyst at 600 °C. The sample was then exposed to 3 vol% NH_3/He (25 mL/min) at ambient temperature. The catalyst was thoroughly purged with pure helium at a rate of 25 mL/min until a consistent baseline was achieved. The catalyst was heated to 550 °C at a rate of 10 °C/min and held for an hour. The temperature at which NH_3 was absorbed on acid sites represents the catalyst's acid strength. Desorption bands below 200 °C, 200–400 °C, and 400–600 °C are from the desorption of adsorbed ammonia on weak, medium, and strong acid sites, respectively [38,39].

2.2.5. Dehydration of sorbitol

Catalytic reactions were performed in a 25 mL Parr autoclave reactor with temperature and agitator controllers. The 10 mL of aqueous sorbitol (5 wt% in water; otherwise noted) was introduced into the reactor using 10 wt% catalyst loading with respect to the reactant. The reactor was purged with nitrogen to remove air and heated to the desired temperature at a constant stirring of 600 rpm. The reaction was stopped by quenching in a water bath. The solution was centrifuged, and the residual solids were removed. The liquid sample was then analyzed using high-performance liquid chromatography (HPLC, Agilent Technology, USA) to measure the concentration of sorbitol and dehydration products.

2.2.6. Product analysis and quantification

The reaction products and remaining reactants were analyzed by HPLC equipped with a refractive index detector (RID) and diode array detector (DAD). The Aminex HPX-87H column (300 x 7.8 mm, Bio-Rad®, USA) was used for separation of reaction products (sorbitol, isosorbide, 1,4-, 1,5-, and 2,5-sorbitans) at 60 °C with 0.6 mL/min 4 mM H_2SO_4 as a mobile phase. The concentrations of feed and products were determined by the peak area from the RID signals (**Fig. S1 and Table S2**). Feed and reaction products were calibrated against certified standards (Absolute Standards, Inc., Hamden, CT, USA). The sorbitol conversion, product yield, and product selectivity were calculated as follows:

$$\text{Sorbitol conversion (\%)} = \frac{\text{sorbitol converted (mol)}}{\text{initial sorbitol (mol)}} \times 100\%$$

$$\text{Product yield (\%)} = \frac{\text{product generated (mol)}}{\text{initial sorbitol (mol)}} \times 100\%$$

$$\text{Product selectivity (\%)} = \frac{\text{product yield (\%)}}{\text{sorbitol conversion (\%)}} \times 100\%$$

2.2.7. Catalyst stability and reusability tests

The stability of catalysts was measured by vacuum filtration of the reaction mixture after performing reactions at 220 °C for 2 h. The vacuum filtration was performed using a 0.2 μm Whatman™ nylon membrane filter (VWR, USA) to separate the solid catalyst from liquid reaction products. The resulting filtrate was then subjected to: (1) HPLC analysis for product examination, and (2) continuing reaction by heating the filtrate to 220 °C without added catalysts and sampling the reaction mixture to determine reaction products. The recovered catalyst was washed with 20 mL DI water and separated by centrifugation twice to remove residual reactant and reaction products. In preparation for the stability assessment, the recovered catalyst was dried overnight in a convection oven at 120 °C. The catalyst recovery was ~85–90 %.

2.2.8. Determination of Brønsted acid site strength of catalysts by polarization method in methanol

The Brønsted acid strengths of solid catalysts were determined by measuring the pH change of methanol in which catalysts were suspended, as described [40,41]. Briefly, 8 mg solid catalysts was suspended in 24 mL methanol with constant stirring at ambient temperature before pH measurement. The pH was measured by a pH electrode with automatic temperature compensation (HI6221, Hanna Instruments, USA). The selected sample amount of 8 mg was based on previous experiments in which the amount of catalysts was varied; we found that 8 mg solid was sufficient such that the measured pH was independent of the solid amount. The pH was measured with a gel-filled, double junction electrode (Milwaukee Instruments, Inc., USA). The electrode was calibrated with the pH 4, 7, and 10 calibration solutions (Hanna Instruments, USA). All measurements were conducted in triplicate.

3. Results

To determine the relation between active sites and catalytic performance of amorphous silica-alumina catalysts (ASA) for conversion of aqueous sorbitol, we characterized the physicochemical and acidic properties of ASA with 5, 30, and 40 wt% silica. We refer to these catalysts as ASA5, ASA30, and ASA40. Then, we correlated the ASA acid properties with their catalytic performance to identify the functions of active sites.

3.1. Physiochemical properties and acid properties of amorphous silica-alumina catalysts

To assess the surface properties of the catalysts, we conducted N_2 adsorption–desorption on ASA5, ASA30, and ASA40. We used γ-Al_2O_3 and SiO_2 as controls. All catalysts had an 8–10 nm pore diameter, indicating their mesoporous structure (**Table S3**). The N_2-adsorption–desorption of all catalytic materials showed Type IV isotherms (**Fig. S2A**). The γ-Al_2O_3 had a specific surface area of 197 m^2/g, a pore volume of 0.52 cm^3/g, and an average pore diameter of 8 nm. The SiO_2 had a surface area of 445 m^2/g, pore volume of 0.76 cm^3/g, and pore diameter of 8 nm. For ASA catalysts, an increase in the silica content decreased surface area and increased pore dimensions, i.e., pore volume and pore diameter. ASA40 had the highest silica content with a high pore volume of 0.84 cm^3/g, a pore diameter of 10 nm, and a low surface area of 271 m^2/g compared with ASA5 (331 m^2/g), consistent with previous studies [42–46]. One reason for increased pore volume and pore diameter with increasing silica content was that introducing silica

in ASAs increased the interactions between silanol groups and aluminum species, potentially enlarging pore attributes [47]. Thus, the silica-to-alumina ratio of ASA catalysts controlled the porous structure and surface properties.

Next, we performed X-ray diffraction on these catalysts to characterize their crystal structures (**Fig. S2B**). The XRD pattern of γ-Al_2O_3 showed (311), (400), and (440) planes, which corresponded to γ-Al_2O_3 phase [48]. The XRD pattern of the ASA5 showed characteristic peaks of γ-Al_2O_3. Likewise, the XRD patterns of ASA40 showed weak (400) and (440) planes of γ-Al_2O_3; weaker planes were due to the dilution effect of high silica content in γ-Al_2O_3 matrix. These results indicated that the γ-Al_2O_3 phase was dominant in ASA catalysts.

Acid properties of catalysts influence product selectivity and sorbitol conversion. To determine the acid properties of ASA catalysts, we performed NH_3-temperature programmed desorption (NH_3-TPD), adsorbed pyridine-Diffuse Reflectance Infrared Fourier Transform spectroscopy (pyridine-DRIFT) and dynamic infrared spectroscopy with pyridine adsorption (pyridine-IR). First, we conducted the NH_3-TPD on these catalysts and calculated the total amount of NH_3 uptake (**Fig. S2C** and **Table S4**). As a control, γ-Al_2O_3 exhibited a broad peak within the 100–400 °C range in the NH_3-TPD profile with the total NH_3 uptake of 0.79 mmol NH_3/g catalyst and a high medium acid site density, agreeing well with a study by Liu [49]. Introducing silica in ASAs decreased the total acid site and medium acid site densities compared with γ-Al_2O_3 with ASA40 showing the lowest amount of NH_3 uptake of 0.34 mmol NH_3/g catalyst. Although NH_3-TPD confirmed a reduction in total acid site density with increased silica content of ASAs, this technique could not differentiate between Brønsted and Lewis acid sites. To address this, we conducted pyridine-DRIFT.

We performed the pyridine-DRIFT at 220 °C to observe the acid site strength at the reaction temperature (200–260 °C, **Fig. S2D**). As a control, SiO_2 exhibited no discernible acid sites, corroborating the finding of Crépeau et al. [50]. The γ-Al_2O_3 showed a Lewis acid site characteristic peak at 1445 cm^{-1}, similar to a study by Phung et al. [51]. ASA catalysts exhibited peaks characteristic of both Lewis acid sites (LAS) and Brønsted acid sites (BAS), indicating the presence of both BAS and LAS sites. The ASA catalysts with high silica content (ASA30 and ASA40) exhibited a lower intensity LAS characteristic peak and a higher intensity BAS characteristic peak than ASA5 [52]. To quantify the acid site density of our catalysts, we performed dynamic infrared spectroscopy with pyridine adsorption (**Fig. S3**). The pyridine-IR results showed that increased silica content in ASA increased the BAS density and lowered LAS density (**Table S5**), corroborating the pyridine-DRIFT results (**Fig. S2D**). These findings demonstrated that a high silica content of ASA indicated a high BAS density.

3.2. *Effect of silica-alumina ratio of amorphous silica-alumina on conversion of aqueous sorbitol*

To measure the catalytic activity of ASA catalysts, we conducted sorbitol conversion experiments at 220 °C for 2 h. Blank experiment (no added catalyst) did not show sorbitol conversion; thus, aqueous sorbitol was thermally stable at 220 °C (Fig. 2), and dehydration of aqueous sorbitol required catalysts. Heating aqueous sorbitol with catalysts yielded sorbitan isomers and isosorbide. The 1,4-sorbitan was the major sorbitan isomer with a trace of 1,5-sorbitan (<2 % yield, **Table S6**). As a control, Lewis acidic γ-Al_2O_3 yielded 14.8 % 1,4-sorbitan at 22 % sorbitol conversion. As expected, SiO_2 displayed negligible catalytic activity. Among the ASA catalysts, the ASA40 catalyst produced the highest 1,4-sorbitan yield of 42 % at 65 % sorbitol conversion. The increased silica content of ASA catalysts improved the 1,4-sorbitan yield and sorbitol conversion. Simultaneously, an increase in the silica content caused side reactions, as shown by the formation of isosorbide. These results indicated a high (40 wt%) silica in ASA40 improved the specific sorbitol activity. Because ASA40 gave the highest 1,4-sorbitan yield and sorbitol conversion, we investigated the ASA40 catalyst to determine the relationship between acid properties and catalytic function.

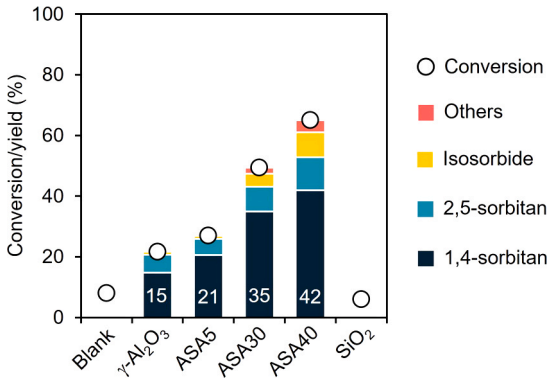

Fig. 2. Sorbitol conversion over investigated catalysts with different SiO_2/Al_2O_3 ratios. Reaction condition: 5 wt% aqueous sorbitol, 220 °C, 2 h, autogenous pressure, 10 wt% catalyst.

3.3. *Effects of reaction conditions on the catalytic performance of silica-alumina catalysts*

To investigate the effect of reaction parameters on the ASA40 catalytic performance, we varied temperature between 200–260 °C (Fig. 3A). The reaction products included 1,4-, 1,5-, and 2,5-sorbitans and isosorbide. The catalytic activity of ASA40 was low at 200 °C. Increasing the reaction temperature enhanced sorbitol conversion. The yield of 1,4-sorbitan had a volcano trend with increasing temperature, reaching a maximum of 42 % at 220 °C with a 65 % sorbitol conversion. We observed a small amount of 1,5-sorbitan (11 %), isosorbide (8 %), and undesired carbonaceous products (4 % coke). At 240 °C, the 1,4-sorbitan yield decreased to 3 % with increases in the amounts of isosorbide (39 %) and undesired coke (47 %). Thus, at a reaction temperature above 220 °C, ASA40 catalyzed the dehydration of 1,4-sorbitan to undesired isosorbide and coke.

To minimize undesired side reactions, we maintained the reaction temperature at 220 °C and assessed the product evolution from the ASA40 catalyst for 24 h (Fig. 3B). We achieved 45 % 1,4-sorbitan yield, at 6 h, the maximum yield, with a complete sorbitol conversion. The 1,4-sorbitan yield progressively decreased after 6 h. This decrease was accompanied by an increase in isosorbide yield, reaching ~55 % after 18 h. As well, the yield of undesired coke progressively increased with time. Thus, ASA40 catalyzed the dehydration of 1,4-sorbitan to isosorbide and coke, a finding that agreed with previous studies [13,38].

To identify the functions of the Lewis and Brønsted acid sites of the ASA40 catalyst, we plotted sorbitan and isosorbide selectivity as a function of sorbitol conversion (Fig. 4). We used γ-Al_2O_3 and Hβ(20) zeolite (Si/Al molar ratio of 20) for comparisons. We chose γ-Al_2O_3 because it was a solid Lewis acidic catalyst. We selected Hβ(20) as a proxy for a solid acid catalyst because Hβ zeolite with 40 wt% silica (0.9Si/Al molar ratio) was not currently attainable. Moreover, Zapata et al. [53] showed that the Hβ zeolites with a high silica content had a high hydrophobicity, which minimized the loss of crystallinity in aqueous reactions at high temperatures. The ASA40 showed the highest sorbitan selectivity across all conversions, followed by Hβ(20) and γ-Al_2O_3 (Fig. 4A**)**. Although γ-Al_2O_3 yielded a high sorbitan selectivity of 68 % at a low conversion of aqueous sorbitol (22 %), an increase in sorbitol conversion by increasing catalyst loading induced the formation of undesired coke (**Fig. S4**). In the case of Hβ(20), an increase in sorbitol conversion led to an increase in the selectivity of undesired isosorbide (Fig. 4B and Fig. S5). These results indicated that the combined effects between Brønsted and Lewis acid sites were essential to improve 1,4-sorbitan selectivity and sorbitol conversion.

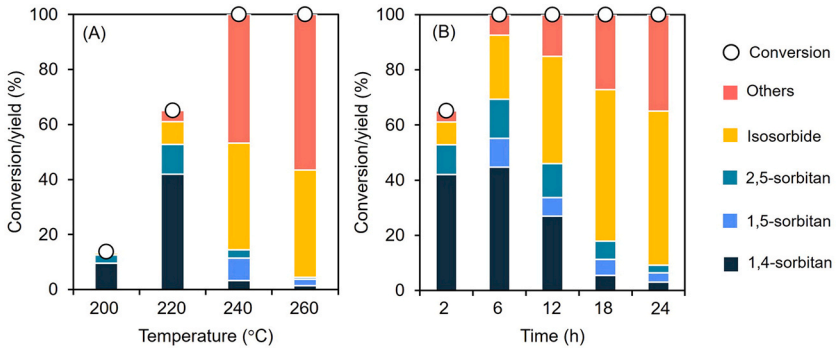

Fig. 3. Effects of reaction temperature (A) and time (B) on sorbitol conversion by ASA40. Reaction condition: 5 wt% aqueous sorbitol, autogenous pressure, and 10 wt% catalyst. Others include unidentified and polymerized products (e.g., coke and humin).

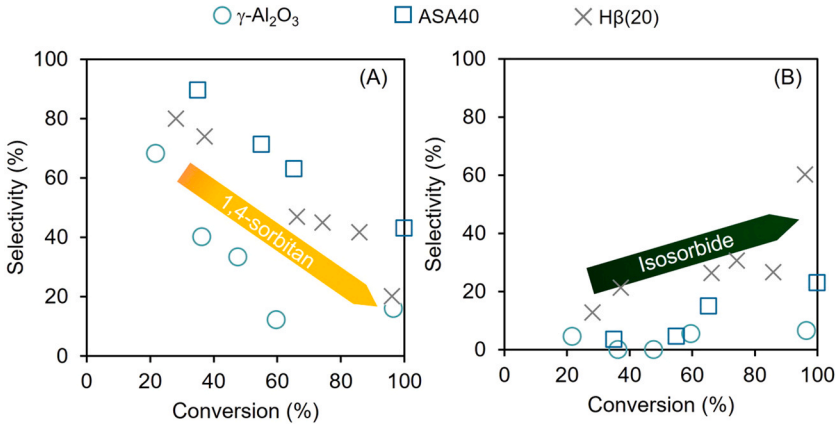

Fig. 4. Selectivity toward 1,4-sorbitan (A) and isosorbide (B) as a function of conversion of aqueous sorbitol by ASA40, Hβ(20), and γ-Al_2O_3. Reaction condition: aqueous sorbitol, 220 °C, and autogenous pressure.

3.4. Recyclability of amorphous silica-alumina catalysts

To assess the stability of the ASA40 catalyst, we conducted a filtration experiment. After reacting at 220 °C for 2 h, we filtered the ASA40 from the reaction mixture. Then, we heated the filtrate under the same reaction condition for an additional 22 h (Fig. 5A). The sorbitol conversion and selectivity toward 1,4-sorbitan and isosorbide remained relatively constant, indicating an absence of catalyst leaching. Next, we recovered the used ASA40 catalyst, washed it with water to remove the residual reactants and products, and dried it at 120 °C overnight before reuse. The used ASA40 catalyst maintained catalytic performance for 4 reuse cycles with < 5 % drop in sorbitol conversion and sorbitan selectivity (Fig. 5B). Thus, the active sites of ASA40 were stable. Given the similar catalytic performance of Hβ(20) to ASA40 (Fig. 4A), we evaluated the reusability of Hβ(20) under the same condition. The used Hβ(20) showed a progressive decrease in sorbitol conversion and selectivity to undesired isosorbide after each reuse cycle (**Fig. S6**), which suggested a progressive deactivation of Hβ(20). However, calcination restored the catalytic activity and selectivity of Hβ(20), which suggested the deactivation in Hβ(20) resulted from coke accumulation and calcination mitigated the deactivation. These results demonstrate ASA40's superior recyclability and stability, with minimal coke formation, making it a more robust catalyst than Hβ(20).

3.5. Hydrothermal stability of amorphous silica-alumina catalysts

The hydrothermal stability of ASA catalysts is critical to retain their acid properties. The hot water can hydrolyze Si-O-Al bonds in ASAs and reduce surface area and porous structure [54]. To determine whether catalysts had incurred structural change under hydrothermal conditions, we treated catalysts by heating them in water without reactant under the experimental condition (220 °C for 2 h) and characterized treated catalysts by X-ray diffraction, FTIR, and Raman spectroscopy. The treated γ-Al_2O_3 and ASA5 showed the reflections of γ-Al_2O_3 and pseudo-boehmite (AlOOH) (**Fig. S7**), which indicated the phase transformation of γ-Al_2O_3 during the reaction. However, we did not observe the pseudo-boehmite phase in the treated ASA40.

Consistent with XRD results, the FTIR bands of used γ-Al_2O_3 and ASA5 exhibited a distinct peak at 1063 cm^{-1} from (OH)-Al=O asymmetric stretching vibration and 810, 762, 588, 555, and 463 cm^{-1} from Al-O stretching vibrations in the distorted AlO_6 of pseudo-boehmite (**Fig. S8A**) [55]. In addition, the Raman shifts of treated γ-Al_2O_3 and ASA5 showed bands at 302, 341, and 478 cm^{-1} from the vibration of Al-O bonds in the AlO_4 and AlO_6 of pseudo-boehmite (**Fig. S8B**) [56,57], consistent with FTIR spectra. Whereas, we did not observe the pseudo-boehmite phase in treated ASA40. These results suggested that the high silica content in ASA40 enhanced hydrothermal stability.

Surface properties of porous catalysts are important in the distribution of active sites and diffusion of molecules in and out of the porous structure. Thus, we measured the surface areas of the treated catalysts to identify changes in surface properties (**Fig. S9**). The treated γ-Al_2O_3 showed a decrease in the surface area from 197 to 122 m^2/g and pore volume from 0.52 to 0.39 cm^3/g with a slight increase in pore diameter from 8 to 10 nm (**Fig. S10 and Table S7**). Likewise, we observed decreased surface area from 331 to 146 m^2/g and pore volume from 0.66 to 0.37 cm^3/g of treated ASA5. Consistent with a study by Mo et al. [48], this decrease in surface area and pore volume of treated γ-Al_2O_3 and ASA5 catalysts indicated the transformation of γ-Al_2O_3 to pseudo-boehmite phase, which corroborated our XRD, FTIR, and Raman results (**Figs. S7** and **S8**). Interestingly, the treated ASA40 catalyst

retained the surface area with a slight decrease in pore volume and diameter, suggesting that the high silica content (40 wt%) of ASA40 improved its hydrothermal stability.

Further, we compared the pyridine-DRIFT spectra of fresh and treated catalysts to assess whether changes occurred in acid types under hydrothermal conditions. The fresh γ-Al_2O_3 exhibited LAS characteristic peak at 1450 cm^{-1} (**Fig. S11**). However, this LAS peak of the treated γ-Al_2O_3 had a lower intensity compared with the fresh γ-Al_2O_3. Likewise, we observed a lower LAS peak intensity in the treated ASA5 compared with fresh ASA5. The treated ASA40 catalysts revealed both LAS and BAS characteristic peaks. Interestingly, the relative LAS peak location and intensity of treated ASA40 remained unchanged compared with the fresh ASA40 catalyst, with a slight decrease in BAS peak intensity. These results suggested that the formation of the pseudo-boehmite phase in treated γ-Al_2O_3 and ASA5 changed the LAS environment and decreased the LAS density.

Because the formation of the pseudo-boehmite phase in γ-Al_2O_3 and ASA5 occurred during the reaction, we sought to evaluate its impact on catalytic performance. We used the treated γ-Al_2O_3 and ASA5 to convert aqueous sorbitol. The treated γ-Al_2O_3 and ASA5 catalysts showed little to no conversion (**Fig. S12**). These results suggested that the pseudo-boehmite phase was inactive for converting aqueous sorbitol.

3.6. Characterization of used catalysts

To determine the types and amounts of coke deposit, we used thermogravimetric analysis (TGA) to characterize the used catalysts after sorbitol conversion. The TGA profiles of the used catalysts showed the presence of two classes of coke: soft cake and hard coke [58]. The soft coke is oxidized between 180–330 °C and can cause the loss of selectivity of desired products. However, the soft coke can be easily removed. Hard coke is oxidized at a higher temperature, 330–700 °C [59], it is carbon-rich, and it can block accessibility to active sites. The used ASA40 catalyst showed 10 % coke formation, composed of 4 % soft coke and 6 % hard coke (**Fig. S13A**). The TGA profile of used Hβ(20) showed 19 % coke formation, 4 % soft coke and 15 % hard coke, an amount 2-fold greater than that associated with used ASA40. The used γ-Al_2O_3 showed ~17 % weight loss after 700 °C from the dehydration of the pseudo-boehmite phase to γ-Al_2O_3 (~11 %) and coke deposition (6 %, **Fig. S13B**). The dehydration of pseudo-boehmite to γ-Al_2O_3 occurred ~450 °C [60]. The 11 % weight loss from this dehydration was lower than the theoretical value (15 %) [61] because the used γ-Al_2O_3 was not completely pseudo-boehmite, consistent with the XRD (**Fig. S7**). These results suggested that, although coke formation in acid catalysts was unavoidable, the amount of coke formed on used ASA40 was low compared with that on used Hβ(20) and γ-Al_2O_3 catalyst.

Characterization techniques for acid properties of solid catalysts, such as NH_3-TPD, pyridine-DRIFT, and pyridine-IR, are performed in the gas phase [62]. These techniques may not accurately represent the acid site strength of catalysts under liquid-phase reaction conditions [62,63] because solvent molecules in liquid media can alter acid strength and affect catalytic performance [64]. Therefore, we used potentiometric titrations to determine the BAS strength of catalysts by measuring the pH change of methanol after suspending catalysts (**Table S8**). A decreased pH value of methanol with suspended catalyst indicates that the catalyst polarizes methanol and has high BAS strength [40]. Because this reaction used a water medium, we further assessed the dependence of catalyst hydration on its BAS strength. We dehydrated catalysts by placing the catalysts in a vacuum oven at 80 °C for 16 h to remove the moisture. We created hydrated catalysts by leaving them in the open atmosphere at 25 °C for 4 days. The pH of methanol with suspensions of hydrated and dehydrated γ-Al_2O_3 was the same as methanol (blank), which suggested that γ-Al_2O_3 possessed only Lewis acidity, consistent with our pyridine-DRIFT results (**Fig. S11**). Conversely, the suspension of dehydrated ASA40 in methanol decreased pH from 6.3 to 4.0, indicating that the silica content in ASA40 enhanced the BAS strength. The suspension of hydrated ASA40 in methanol showed a slightly higher pH than that of dehydrated ASA40 (Fig. 6), indicating that bound water molecules lowered the Brønsted acid strength. After removing the hydrated ASA40, the pH of methanol was ~6.3, which suggested that the Brønsted acidic proton was on the surface of ASA40. Interestingly, the used hydrated ASA40 had a pH of 4.4, a slightly greater value than that of fresh hydrated ASA40 (4.2), suggesting that coke formed on used ASA40 slightly reduced the BAS strength.

Zeolites have stronger BAS strength compared with ASAs [25,65]. The high BAS strength can enhance catalytic activity but also promote over-dehydration reactions, leading to unwanted by-products such as isosorbide and increased coke formation. Because we observed a high isosorbide selectivity and coke formation with Hβ(20), we postulated that the high BAS strength of Hβ(20) facilitated the over-dehydration of 1,4-sorbitan to isosorbide. The dehydrated Hβ(20) suspension in methanol decreased pH from 6.3 to 2.4. The suspension of hydrated Hβ(20) caused the pH to increase to 2.7, which implied that bound water decreased the Brønsted acid strength of Hβ(20). The pH of hydrated Hβ(20) in methanol was lower than that of ASA40 in methanol (4.2), suggesting that Hβ(20) had a higher BAS strength compared with ASA40, in agreement with previous studies [25,26]. The used Hβ(20) produced a higher pH than fresh Hβ(20), indicative of a loss in Brønsted acid strength (Fig. 6). Thus, we inferred that the coke formed on used Hβ(20) reduced BAS strength. This decrease in BAS strength of used Hβ(20) lowered the isosorbide yield/selectivity (**Fig. S6**). These results suggested a high BAS strength facilitated further sorbitan dehydration to isosorbide and coke formation.

To measure changes in physical properties, we conducted N_2-adsorption/desorption of used ASA40 and Hβ(20). The used Hβ(20) had a surface area of 424 m^2/g and pore volume of 0.30 cm^3/g, lower values than fresh Hβ(20) (**Fig. S14 and Table S7**). Whereas, the used ASA40 showed a slight decrease in surface area (236 m^2/g) and pore volume (0.58 cm^3/g) compared with fresh catalysts (271 m^2/g and 0.84 cm^3/g). These results suggested that a strong BAS of Hβ(20) facilitated coke formation, which decreased the accessibility to acid sites.

We further characterized the used catalysts by pyridine-DRIFT to determine changes in acid site densities due to coke deposition. The used Hβ(20) showed a significant decrease in BAS and LAS intensity compared with the fresh Hβ(20) (**Fig. S15**). The used Hβ(20) lost both BAS and LAS characteristics after 3 reuse cycles, consistent with the potentiometric titration results (Fig. 6). Moreover, the calcined Hβ(20) recovered its LAS and BAS characteristics (**Fig. S15A**) and catalytic performance (**Fig. S6**). These results suggested that coke blocked accessibility to the LAS and BAS of Hβ(20). Conversely, used ASA40 catalysts showed a relatively strong LAS peak with only a slight decrease in relative BAS peak even after the 4th reuse cycle (**Fig. S15B**), indicating high LAS and BAS accessibility. These results further confirmed that the optimal BAS strength of ASA40 minimized coke formation and improved 1,4-sorbitan selectivity.

3.7. Catalyst property-function relationships

In Fig. 7, we propose a reaction pathway for conversion of aqueous sorbitol by LAS and BAS on ASA40. This reaction involved a single dehydration step of sorbitol conversion to 1,4-sorbitan by LAS and/or BAS. BAS on ASA40 had terminal silanol groups activated by the nearest aluminum ions [66]. As a result, the BAS had less steric hindrance than the coordinated unsaturated Al^{3+} ions that acted as LAS [66]. The BAS protonated the hydroxyl group at the C_1 position of sorbitol. Then 1,4-cyclization occurred at C_4 to yield 1,4-sorbitan. Although BAS on ASA catalysts facilitated the formation of 1,4-sorbitan, the high BAS strength promoted dehydration of 1,4-sorbitan to undesired isosorbide and degradation of isosorbide to coke [13,67,68]. Therefore, we postulated that the localized LAS-BAS pair in ASA40 induced the optimal BAS strength and minimized the conversion of 1,4-sorbitan to isosorbide.

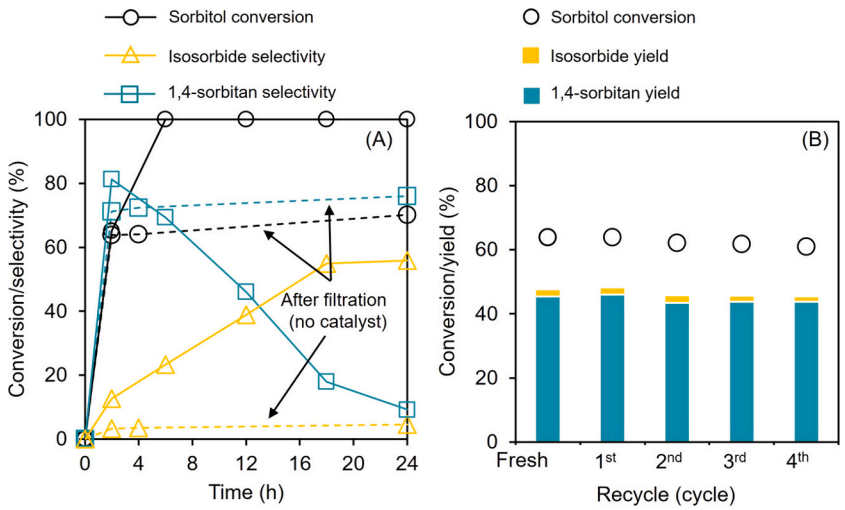

Fig. 5. Catalyst filtration test and reusability of ASA40. The filtration test after 2 h at 220 °C (A) and reusability test (B). Reaction condition: 5 wt% aqueous sorbitol, 220 °C, 2 h, autogenous pressure, 10 wt% catalyst. Dash lines indicate results from filtration experiments.

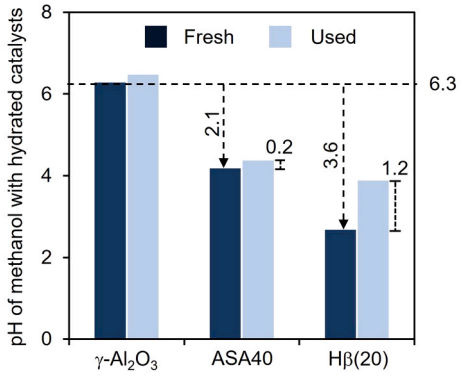

Fig. 6. pH values of methanol with suspension of the fresh and used catalysts.

4. Discussion

We have deduced the structure–function relationship of amorphous silica-alumina (ASA) for selective conversion of aqueous sorbitol to 1,4-sorbitan. Having both Lewis acid sites (LAS) and Brønsted acid sites (BAS) makes ASA catalysts versatile in biomass conversion reactions [69] because the combination of sites favors selective dehydration and prevents excessive polymerization, enabling controlled conversion of aqueous sorbitol to 1,4-sorbitan. However, the function of acid properties of ASA catalysts in aqueous sorbitol conversion was unclear. Here, we demonstrated that silica incorporation in the γ-Al_2O_3 matrix of ASA catalysts gave two functions: (1) preventing phase transformation of γ-Al_2O_3 matrix and (2) providing optimal BAS strength, which minimized over-dehydration and degradation of the desired product 1,4-sorbitan. The ASA40 (with 40 wt% silica) yielded a high 1,4-sorbitan selectivity of 65 % at 65 % conversion of aqueous sorbitol. Our findings pinpoint the importance of the localized BAS-LAS pair and their acid strengths for the selective production of 1,4-sorbitan from aqueous sorbitol.

Our most significant finding is that the 40 wt% silica in ASA catalysts prevented the phase transformation of γ-Al_2O_3. The stability of the γ-Al_2O_3 phase ensured that the Lewis acid site (LAS) density and strength were retained. This retention prevented loss of activity and selectivity in high-temperature aqueous reactions, consistent with the findings of Van Cleve et al. [70] and Sudheer et al. [61]. For ASA, the incorporation of silica in γ-Al_2O_3 matrix formed the Si-O-Al framework, reducing the availability of Al sites and minimizing the formation of pseudo-boehmite. The 5 wt% silica in the ASA5 catalyst was insufficient to protect the phase transformation of γ-Al_2O_3 matrix into an inactive pseudo-boehmite phase; thus ASA5 lost surface area, pore volume, and LAS strength (**Figs. S10 and S11**). We found that 40 wt% silica in the ASA40 catalyst maintained its surface area, pore characteristics, and acid properties and prevented the formation of inactive pseudo-boehmite phase under the experimental condition. As a result, the ASA40 catalyst maintained its catalytic activity and sorbitan selectivity for at least four use cycles (Fig. 5).

Another significant finding is that the BAS and optimal BAS strength of ASA40 minimized the dehydration of the desired product, 1,4-sorbitan, and minimized coke formation. To decouple the contribution of LAS and BAS, we let LAS act independently in the dehydration of aqueous sorbitol. We demonstrated that γ-Al_2O_3 exhibited only LAS and was selective to 1,4-sorbitan, which agreed with the findings of Guo et al. [67] in a study of Lewis acidic $AlCl_3$ catalysts. However, LAS of γ-Al_2O_3 facilitated 1,4-sorbitan polymerization to undesired coke (**Fig. S4**) [71]. BAS in ASA40 protected 1,4-sorbitan from LAS-mediated

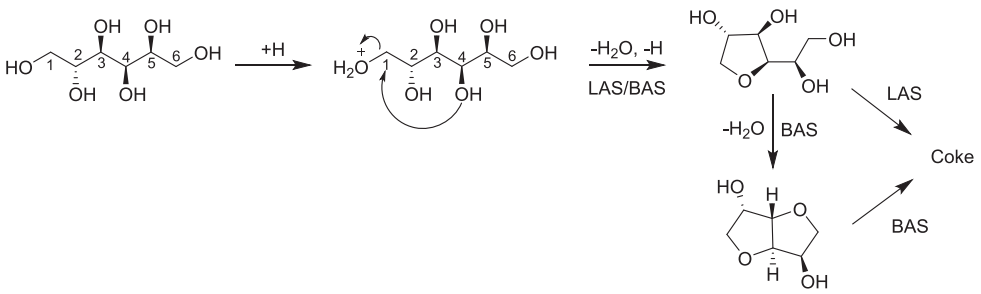

Fig. 7. Proposed reaction mechanism of sorbitol conversion by Lewis acid sites (LAS) and Brønsted acid sites (BAS).

polymerizing of coke, as shown in a high 1,4-sorbitan selectivity of 90 % and ability to reuse ASA40 (Fig. 5).

Moreover, the optimal BAS strength of ASA40 minimized the further dehydration of 1,4-sorbitan to isosorbide. For comparison, we used Hβ (20), which had a higher BAS strength compared with ASA40 (Fig. 6). The high BAS strength of Hβ(20) catalyst led to over-dehydration of 1,4-sorbitan to isosorbide and coke formation, as shown by an increase in undesired isosorbide selectivity and coke (**Figs. S6 and S13**). Our findings agreed well with studies that showed that a high BAS strength of zeolites promoted side reactions of 1,4-sorbitan dehydration to isosorbide and coke formation [13,72]. These results agreed well with the findings by Flèche and Huchette [8], who showed that acid catalysts with medium acid strength catalyzed the conversion of aqueous sorbitol to sorbitan in high yield.

Our findings advance the understanding of amorphous silica-alumina catalysts for selective conversion of aqueous sorbitol to 1,4-sorbitan. Previous studies (**Table S9** and **Fig. S16**) [4,12–18] using catalysts with a high BAS strength, such as Hβ zeolites, showed undesired dehydration of 1,4-sorbitan to isosorbide. Our work demonstrated that the ASA40 catalyst offered a balanced acidity that enhanced the selectivity of 1,4-sorbitan while maintaining stability under hydrothermal conditions. The stable acid properties in aqueous reaction systems and tunable acid properties of amorphous silica-alumina catalysts can be extended to other aqueous biomass conversion systems, including isomerization, acetalization, hydrolysis, esterification, and condensation.

5. Conclusions

We present an active and selective catalytic system for the conversion of aqueous sorbitol to 1,4-sorbitan by amorphous silica-alumina catalysts, offering improved stability and selectivity compared with conventional mineral acid and zeolite-based systems. Incorporating silica in the γ-Al_2O_3 matrix in amorphous silica-alumina enhanced hydrothermal stability and optimal Brønsted acid sites (BAS) strength. The hydrothermal stability of amorphous silica-alumina catalyst with 40 wt % silica prevented the phase transformation. Avoiding phase transformation is critical for maintaining long-term catalyst efficiency by preserving active acid sites and preventing structural degradation, ensuring sustained catalytic performance. The optimal BAS strength of ASA40 minimized the desired 1,4-sorbitan from over-dehydration to isosorbide and degraded into coke. As a result, the amorphous silica-alumina catalyst maintained its catalytic performance and was reusable after recycling four times. These results underscore the hydrothermal stability and medium BAS strength for maximizing the 1,4-sorbitan formation and minimizing the subsequent dehydration/degradation. The mechanistic understanding gained from this work reveals that the interplay between Brønsted and Lewis acid sites, along with controlled silica incorporation, is essential for stabilizing catalytic activity and selectivity. This knowledge will guide the design of selective solid acid catalysts to 1,4-sorbitan production. Future studies will focus on investigating the effects of silica content on the degree of hydrothermal stability and acid properties for aqueous reactions.

CRediT authorship contribution statement

Napat Lertthanaphol: Writing – original draft, Investigation, Formal analysis. **Pakawan Sereerattanakorn:** Investigation, Formal analysis. **Sarttrawut Tulaphol:** Visualization, Formal analysis. **Thana Maihom:** Methodology, Investigation, Formal analysis, Conceptualization. **Thanh Khoa Phung:** Writing – original draft, Investigation, Conceptualization. **Gabriella Garbarino:** Writing – review & editing, Supervision, Methodology, Conceptualization. **Guido Busca:** Writing – review & editing, Supervision, Methodology, Conceptualization. **Jatuporn Wittayakun:** Supervision, Funding acquisition. **Vance Jaeger:** Validation, Formal analysis. **Shashi B. Lalvani:** Writing – original draft, Conceptualization. **Noppadon Sathitsuksanoh:** Writing – review & editing, Writing – original draft, Supervision, Project administration, Funding acquisition, Conceptualization.

Declaration of competing interest

The authors declare the following financial interests/personal relationships which may be considered as potential competing interests: Noppadon Sathitsuksanoh reports financial support was provided by National Science Foundation. If there are other authors, they declare that they have no known competing financial interests or personal relationships that could have appeared to influence the work reported in this paper.

Acknowledgment

The authors thank Drs. Marcos Schöneborn and Luke Tatum at Sasol for providing silica-alumina materials. The authors would like to thank the Conn Center for Renewable Energy Research at the University of Louisville for its support in the material characterization. The authors thank E. Finocchio and R.P.P. Vijayakumar at the University of Genova for performing the dynamic IR spectroscopy and Sasikarn Liengpornpattana and Sarnrak Ratanapantowong from Thammasat University for conducting the FTIR spectroscopy.

Appendix A. Supplementary data

Supplementary data to this article can be found online at https://doi.org/10.1016/j.cej.2025.161918.

Data availability

Data will be made available on request.

References

[1] T. Cottrell, J. Peij, Sorbitan esters and polysorbates, in: V. Norn (Ed.), Emulsifiers in Food Technology, John Wiley & Sons Ltd, 2014, pp. 271–296.
[2] B.A. Kerwin, Polysorbates 20 and 80 used in the formulation of protein biotherapeutics: structure and degradation pathways, J. Pharm. Sci. 97 (8) (2008) 2924–2935, https://doi.org/10.1002/jps.21190.
[3] W.L. Kubie, J.L. O'Donnell, H.M. Teeter, J.C. Cowan, Emulsifiers derived from linseed oil and their potential use in coatings, J. Am. Oil Chem. Soc. 40 (3) (1963) 105–107, https://doi.org/10.1007/BF02640700.
[4] I. Bonnin, R. Méreau, T. Tassaing, K. Oliveira Vigier, Selective one-pot synthesis of sorbitans (1,4-sorbitan and 3,6-sorbitan) from glucose via catalytic hydrogenation and CO_2-mediated dehydration, ACS Sustain. Chem. Eng. 12 (19) (2024) 7276–7288, https://doi.org/10.1021/acssuschemeng.3c08156.
[5] EFSA FEEDAP, V. Bampidis, G. Azimonti, M. Bastos, H. Christensen, B. Dusemund, M. Kos Durjava, M. Kouba, M. López-Alonso, S. López Puente, F. Marcon, B. Mayo, A. Pechová, M. Petkova, F. Ramos, Y. Sanz, R.E. Villa, R. Woutersen, G. Bories, A. Finizio, A. Focks, I. Teodorovic, P. Manini, J. Tarrés-Call, Safety for the environment of sorbitan monolaurate as a feed additive for all animal species, EFSA J 18 (6) (2020) e06162, https://doi.org/10.2903/j.efsa:2020.6162.
[6] S. Murdan, G. Gregoriadis, A.T. Florence, Novel sorbitan monostearate organogels, J. Pharm. Sci. 88 (6) (1999) 608–614, https://doi.org/10.1021/js980342r.
[7] N. Li, G. Huber, Aqueous-phase hydrodeoxygenation of sorbitol with Pt/SiO_2–Al_2O_3: Identification of reaction intermediates, J. Catal. 270 (1) (2010) 48–59, https://doi.org/10.1016/j.jcat.2009.12.006.
[8] G. Flèche, M. Huchette, Isosorbide. Preparation, properties and chemistry, Starch/Stärke 38 (1) (1986) 26–30, https://doi.org/10.1002/star.19860380107.
[9] M. Yabushita, H. Kobayashi, A. Shrotri, K. Hara, S. Ito, A. Fukuoka, Sulfuric acid-catalyzed dehydration of sorbitol: mechanistic study on preferential formation of 1,4-sorbitan, Bull. Chem. Soc. Jpn. 88 (7) (2015) 996–1002, https://doi.org/10.1246/bcsj.20150080.
[10] A.A. Dabbawala, D.K. Mishra, G.W. Huber, J.S. Hwang, Role of acid sites and selectivity correlation in solvent free liquid phase dehydration of sorbitol to isosorbide, Appl. Catal. A Gen. 492 (2015) 252–261, https://doi.org/10.1016/j.apcata.2014.12.014.
[11] M. Belluati, S. Tabasso, F. Bucciol, T. Tabanelli, F. Cavani, G. Cravotto, M. Manzoli, Sustainable isosorbide production by a neat one-pot MW-assisted catalytic glucose conversion, Catal. Today 418 (2023) 114086, https://doi.org/10.1016/j.cattod.2023.114086.

[12] M. Caiti, G. Tarantino, C. Hammond, Developing a continuous process for isosorbide production from renewable sources, ChemCatChem 12 (24) (2020) 6393–6400, https://doi.org/10.1002/cctc.202001278.
[13] F. Brandi, I. Khalil, M. Antonietti, M. Al-Naji, Continuous-flow production of isosorbide from aqueous-cellulosic derivable feed over sustainable heterogeneous catalysts, ACS Sustain. Chem. Eng. 9 (2) (2020) 927–935, https://doi.org/10.1021/acssuschemeng.0c08167.
[14] F. Brandi, M. Al-Naji, Sustainable sorbitol dehydration to isosorbide using solid acid catalysts: transition from batch reactor to continuous-flow system, ChemSusChem 15 (5) (2022) e202102525, https://doi.org/10.1002/cssc.202102525.
[15] R. Otomo, T. Yokoi, T. Tatsumi, Synthesis of isosorbide from sorbitol in water over high-silica aluminosilicate zeolites, Appl. Catal. A Gen. 505 (2015) 28–35, https://doi.org/10.1016/j.apcata.2015.07.034.
[16] Z.C. Tang, D.H. Yu, P. Sun, H. Li, H. Huang, Phosphoric acid modified Nb_2O_5: A selective and reusable catalyst for dehydration of sorbitol to isosorbide, Bull. Korean Chem. Soc. 31 (12) (2010) 3679–3683, https://doi.org/10.5012/bkcs.2010.31.12.3679.
[17] K. Zhang, K. Wang, X. Wang, Catalytic dehydration of sorbitol to isosorbide over sulfonated phenolic resins with surface hydrophobic modification, New J. Chem. 48 (19) (2024) 8860–8867, https://doi.org/10.1039/D4NJ00351A.
[18] M. Boupan, P. Wongpakham, O. Sabangban, A. Neramittagapong, S. Theerakulpisut, S. Neramittagapong, Catalytic performance of acid catalysts for sorbitol dehydration to isosorbide, J. Jpn. Inst. Energy 100 (10) (2021) 206–211, https://doi.org/10.3775/jie.100.206.
[19] M.R. Kamaruzaman, X.X. Jiang, X. De Hu, S.Y. Chin, High yield of isosorbide production from sorbitol dehydration catalysed by Amberlyst 36 under mild condition, Chem. Eng. J. 388 (2020) 124186, https://doi.org/10.1016/j.cej.2020.124186.
[20] D. Yuan, F. Xiao, N. Zhao, C. Deng, X. Huang, H. Zhang, Q. Yang, Y. Qiao, Mesoporous poly (ionic liquid) solid acid for sequential dehydration of sorbitol to isosorbide, Chem. Eng. J. 460 (2023) 141780, https://doi.org/10.1016/j.cej.2023.141780.
[21] I. Polaert, M.C. Felix, M. Fornasero, S. Marcotte, J.C. Buvat, L. Estel, A greener process for isosorbide production: Kinetic study of the catalytic dehydration of pure sorbitol under microwave, Chem. Eng. J. 222 (2013) 228–239, https://doi.org/10.1016/j.cej.2013.02.043.
[22] D. Yuan, N. Zhao, Y. Wang, K. Xuan, F. Li, Y. Pu, F. Wang, L. Li, F. Xiao, Dehydration of sorbitol to isosorbide over hydrophobic polymer-based solid acid, Appl. Catal. B 240 (2019) 182–192, https://doi.org/10.1016/j.apcatb.2018.08.036.
[23] X. Zhang, A.I.M. Rabee, M. Isaacs, A. Lee, K. Wilson, Sulfated zirconia catalysts for D-sorbitol cascade cyclodehydration to isosorbide: Impact of zirconia phase, ACS Sustain. Chem. Eng. 6 (11) (2018) 14704–14712, https://doi.org/10.1021/acssuschemeng.8b03268.
[24] K. Larmier, C. Chizallet, S. Maury, N. Cadran, J. Abboud, A.F. Lamic-Humblot, E. Marceau, H. Lauron-Pernot, Isopropanol dehydration on amorphous silica–alumina: synergy of Brønsted and Lewis acidities at pseudo-bridging silanols, Angew. Chem. Int. Ed. 56 (1) (2017) 230–234, https://doi.org/10.1002/anie.201609494.
[25] D.G. Poduval, J.A.R. Van Veen, M.S. Rigutto, E.J.M. Hensen, Brønsted acid sites of zeolitic strength in amorphous silica-alumina, Chemical Commun 46 (20) (2010) 3466–3468, https://doi.org/10.1039/c000019a.
[26] F. Leydier, C. Chizallet, D. Costa, P. Raybaud, Revisiting carbenium chemistry on amorphous silica-alumina: Unraveling their milder acidity as compared to zeolites, J. Catal. 325 (2015) 35–47, https://doi.org/10.1016/j.jcat.2015.02.012.
[27] G. Busca, Acid catalysts in industrial hydrocarbon chemistry, Chem. Rev. 107 (11) (2007) 5366–5410, https://doi.org/10.1021/cr068042e.
[28] M.K. Mardkhe, B. Huang, C.H. Bartholomew, T.M. Alam, B.F. Woodfield, Synthesis and characterization of silica doped alumina catalyst support with superior thermal stability and unique pore properties, J. Porous Mater. 23 (2) (2016) 475–487, https://doi.org/10.1007/s10934-015-0101-z.
[29] M. Zabeti, T.S. Nguyen, L. Lefferts, H.J. Heeres, K. Seshan, In situ catalytic pyrolysis of lignocellulose using alkali-modified amorphous silica alumina, Biores Technol 118 (2012) 374–381, https://doi.org/10.1016/j.biortech.2012.05.034.
[30] T. Li, Z. Tao, L. Zhang, Y. Yang, Facile and cost-effective synthesis of acidity-enhanced amorphous silica-alumina for high-performance isomerization, J. Solid State Chem. 300 (2021) 122249, https://doi.org/10.1016/j.jssc.2021.122249.
[31] K.S.W. Sing, Reporting physisorption data for gas/solid systems with special reference to the determination of surface area and porosity (Recommendations 1984), Pure Appl. Chem. 57 (4) (1985) 603–619, https://doi.org/10.1351/pac198557040603.
[32] E.P. Barrett, L.G. Joyner, P.P. Halenda, The determination of pore volume and area distributions in porous substances. I. computations from nitrogen isotherms, J. Am. Chem. Soc. 73 (1) (1951) 373–380, https://doi.org/10.1021/ja01145a126.
[33] S.K. Jana, R. Nishida, K. Shindo, T. Kugita, S. Namba, Pore size control of mesoporous molecular sieves using different organic auxiliary chemicals, Microporous Mesoporous Mater 68 (1–3) (2004) 133–142, https://doi.org/10.1016/j.micromeso.2003.12.010.
[34] L. Desmurs, A. Galarneau, C. Cammarano, V. Hulea, C. Vaulot, H. Nouali, B. Lebeau, T. Daou, C. Vieira Soares, G. Maurin, M. Haranczyk, I. Batonneau-Gener, A. Sachse, Determination of microporous and mesoporous surface areas and volumes of mesoporous zeolites by corrected t-plot analysis, ChemNanoMat 8 (4) (2022) e202200051, https://doi.org/10.1002/cnma.202200051.
[35] G. Busca, Spectroscopic characterization of the acid properties of metal oxide catalysts, Catal. Today 41 (1–3) (1998) 191–206, https://doi.org/10.1016/S0920-5861(98)00049-2.
[36] C.A. Emeis, Determination of integrated molar extinction coefficients for infrared absorption bands of pyridine adsorbed on solid acid catalysts, J. Catal. 141 (2) (1993) 347–354, https://doi.org/10.1006/jcat.1993.1145.
[37] A.I. Osman, J.K. Abu-Dahrieh, D.W. Rooney, S.A. Halawy, M.A. Mohamed, A. Abdelkader, Effect of precursor on the performance of alumina for the dehydration of methanol to dimethyl ether, Appl. Catal. B 127 (2012) 307–315, https://doi.org/10.1016/j.apcatb.2012.08.033.
[38] Y. Zhang, T. Chen, G. Zhang, G. Wang, H. Zhang, Mesoporous Al-promoted sulfated zirconia as an efficient heterogeneous catalyst to synthesize isosorbide from sorbitol, Appl. Catal. A Gen. 562 (2018) 258–266, https://doi.org/10.1016/j.apcata.2018.06.024.
[39] J.C. Morales-Ortuño, R.A. Ortega-Domínguez, P. Hernández-Hipólito, X. Bokhimi, T.E. Klimova, HDS performance of NiMo catalysts supported on nanostructured materials containing titania, Catal. Today 271 (2016) 127–139, https://doi.org/10.1016/j.cattod.2015.07.028.
[40] F.G. Cirujano, F.X. Llabrés i Xamena, Tuning the catalytic properties of UiO-66 metal–organic frameworks: from Lewis to defect-induced Brønsted acidity, J. Phys. Chem. Lett. 11 (12) (2020) 4879–4890, https://doi.org/10.1021/acs.jpclett.0c00984.
[41] M.S. Rahaman, S. Tulaphol, M.A. Hossain, M. Mulvehill, J. Spurgeon, T. Maihom, N. Sathitsuksanoh, Mechanism of transfer hydrogenation of carbonyl compounds by zirconium and hafnium-containing metal-organic frameworks, Mol. Catal. 522 (2022) 112247, https://doi.org/10.1016/j.mcat.2022.112247.
[42] P.G. Tsyrul'nikov, T.N. Afonasenko, S.V. Koshcheev, A.I. Boronin, State of palladium in palladium-aluminosilicate catalysts as studied by XPS and the catalytic activity of the catalysts in the deep oxidation of methane, Kinet. Catal. 48 (2007) 728–734, https://doi.org/10.1134/S0023158407050187.
[43] M. Caillot, A. Chaumonnot, M. Digne, J.A. van Bokhoven, The variety of Brønsted acid sites in amorphous aluminosilicates and zeolites, J. Catal. 316 (2014) 47–56, https://doi.org/10.1016/j.jcat.2014.05.002.
[44] A.A. Christy, Quantitative determination of surface area of silica gel particles by near infrared spectroscopy and chemometrics, Colloids Surf., A 322 (1–3) (2008) 248–252, https://doi.org/10.1016/j.colsurfa.2008.03.021.
[45] A. Ishihara, H. Negura, T. Hashimoto, H. Nasu, Catalytic properties of amorphous silica-alumina prepared using malic acid as a matrix in catalytic cracking of n-dodecane, Appl. Catal. A Gen. 388 (1–2) (2010) 68–76, https://doi.org/10.1016/j.apcata.2010.08.027.
[46] V. Meille, S. Pallier, G.V.S.C. Bustamante, M. Roumanie, J.P. Reymond, Deposition of γ-Al_2O_3 layers on structured supports for the design of new catalytic reactors, Appl. Catal. A Gen. 286 (2) (2005) 232–238, https://doi.org/10.1016/j.apcata.2005.03.028.
[47] F. Coumans, B. Mezari, N. Zuidema, J.M.J.J. Heinrichs, E.J.M. Hensen, Isolating Al surface sites in amorphous silica–alumina by homogeneous deposition of Al^{3+} on SiO_2 nanoparticles, ACS Appl. Nano Mater. 7 (22) (2024) 25524–25534, https://doi.org/10.1021/acsanm.4c04544.
[48] Y. Mo, C. Li, H. Li, L.A. Estudillo-Wong, L. Wu, Y. Wang, H. Yu, D. Li, Y. Feng, Hydrothermal stability of gamma-Al_2O_3 supports varied with crystal plane orientation of pseudo-boehmite precursor, Chem. Eng. Sci. 287 (2024) 119705, https://doi.org/10.1016/j.ces.2024.119705.
[49] X. Liu, DRIFTS study of surface of γ-alumina and its dehydroxylation, J. Phys. Chem. C 112 (13) (2008) 5066–5073, https://doi.org/10.1021/jp711901s.
[50] G. Crépeau, V. Montouillout, A. Vimont, L. Mariey, T. Cseri, F. Maugé, Nature, structure and strength of the acidic sites of amorphous silica alumina: an IR and NMR study, J. Phys. Chem. B 110 (31) (2006) 15172–15185, https://doi.org/10.1021/jp062252d.
[51] T.K. Phung, C. Herrera, M.Á. Larrubia, M. García-Diéguez, E. Finocchio, L. J. Alemany, G. Busca, Surface and catalytic properties of some γ-Al_2O_3 powders, Appl. Catal. A Gen. 483 (2014) 41–51, https://doi.org/10.1016/j.apcata.2014.06.020.
[52] Y. Matsunaga, H. Yamazaki, T. Yokoi, T. Tatsumi, J.N. Kondo, IR characterization of homogeneously mixed silica–alumina samples and dealuminated Y zeolites by using pyridine, CO, and propene probe molecules, J. Phys. Chem. C 117 (27) (2013) 14043–14050, https://doi.org/10.1021/jp403242n.
[53] P.A. Zapata, Y. Huang, M.A. Gonzalez-Borja, D.E. Resasco, Silylated hydrophobic zeolites with enhanced tolerance to hot liquid water, J. Catal. 308 (2013) 82–97, https://doi.org/10.1016/j.jcat.2013.05.024.
[54] M.W. Hahn, J.R. Copeland, A.H. Van Pelt, C. Sievers, Stability of amorphous silica–alumina in hot liquid water, ChemSusChem 6 (12) (2013) 2304–2315, https://doi.org/10.1002/cssc.201300532.
[55] S. Bocchini, S. Morlat-Thérias, J.L. Gardette, G. Camino, Influence of nanodispersed boehmite on polypropylene photooxidation, Polym. Degrad. Stab. 92 (10) (2007) 1847–1856, https://doi.org/10.1016/j.polymdegradstab.2007.07.002.
[56] A.B. Kiss, G. Keresztury, L. Farkas, Raman and ir spectra and structure of boehmite (γ-AlOOH): evidence for the recently discarded D_{2h}^{17} space group, Spectrochim. Acta, Part A 36 (7) (1980) 653–658, https://doi.org/10.1016/0584-8539(80)80024-9.
[57] L. Geerts, H. Geerts-Claes, A. Skorikov, J. Vermeersch, G. Vanbutsele, V. Galvita, D. Constales, C. Chandran, S. Radhakrishnan, J. Seo, Spherical core–shell alumina support particles for model platinum catalysts, Nanoscale 13 (7) (2021) 4221–4232, https://doi.org/10.1039/d0nr08456e.
[58] M. Wolf, N. Raman, N. Taccardi, M. Haumann, P. Wasserscheid, Coke formation during propane dehydrogenation over Ga−Rh supported catalytically active liquid

metal solutions, ChemCatChem 12 (4) (2020) 1085–1094, https://doi.org/10.1002/cctc.201901922.
[59] A.R. Pradhan, J.F. Wu, S.J. Jong, T.C. Tsai, S.B. Liu, An ex situ methodology for characterization of coke by TGA and ^{13}C CP-MAS NMR spectroscopy, Appl. Catal. A Gen. 165 (1–2) (1997) 489–497, https://doi.org/10.1016/S0926-860x(97)00231-7.
[60] G. Busca, Chapter Three - Structural, surface, and catalytic properties of aluminas, in: F.C. Jentoft (Ed.), Advances in Catalysis, Academic Press, 2014, pp. 319–404, https://doi.org/10.1016/B978-0-12-800127-1.00003-5.
[61] N. Sudheer, S. Sharna, V. Rouchon, D. Ihiawakrim, M. Lenertz, P. Levitz, P. Rabu, O. Ersen, Evolution of correlated morphological and structural disorder in boehmite-derived alumina with progressive calcination, ChemCatChem 16 (20) (2024) e202400677, https://doi.org/10.1002/cctc.202400677.
[62] N.S. Gould, B. Xu, Effect of liquid water on acid sites of NaY: An in situ liquid phase spectroscopic study, J. Catal. 342 (2016) 193–202, https://doi.org/10.1016/j.jcat.2016.08.008.
[63] K. Yu, N. Kumar, A. Aho, J. Roine, I. Heinmaa, D.Y. Murzin, A. Ivaska, Determination of acid sites in porous aluminosilicate solid catalysts for aqueous phase reactions using potentiometric titration method, J. Catal. 335 (2016) 117–124, https://doi.org/10.1016/j.jcat.2015.12.010.
[64] C. Sievers, Y. Noda, L. Qi, E.M. Albuquerque, R.M. Rioux, S.L. Scott, Phenomena affecting catalytic reactions at solid–liquid interfaces, ACS Catal 6 (12) (2016) 8286–8307, https://doi.org/10.1021/acscatal.6b02532.
[65] F.J.A.G. Coumans, B. Mezari, E.J.M. Hensen, Identifying the role of Brønsted and Lewis acid sites in the Diels-Alder cycloaddition of 2,5-DMF and ethylene, ChemCatChem 16 (2) (2024) e202301216, https://doi.org/10.1002/cctc.202301216.
[66] C. Chizallet, P. Raybaud, Acidity of amorphous silica–alumina: from coordination promotion of Lewis sites to proton transfer, ChemPhysChem 11 (1) (2010) 105–108, https://doi.org/10.1002/cphc.200900797.
[67] J. Guo, Y. Song, S. Liu, L. Huang, X. Wang, C. Li, Sequential dehydration of sorbitol to isosorbide over acidified niobium oxides, Catal. Sci. Technol. 11 (12) (2021) 4226–4234, https://doi.org/10.1039/d1cy00326g.
[68] J.T. Hopper, R. Ma, J.B. Rawlings, P.C. Ford, M.M. Abu-Omar, Markedly improved catalytic dehydration of sorbitol to isosorbide by sol–gel sulfated zirconia: a quantitative structure–reactivity study, ACS Catal. 13 (15) (2023) 10137–10152, https://doi.org/10.1021/acscatal.3c00755.
[69] Z. Wang, T. Li, Y. Jiang, O. Lafon, Z. Liu, J. Trébosc, A. Baiker, J.P. Amoureux, J. Huang, Acidity enhancement through synergy of penta-and tetra-coordinated aluminum species in amorphous silica networks, Nature Commun. 11 (1) (2020) 225, https://doi.org/10.1038/s41467-019-13907-7.
[70] T. Cleve, D. Underhill, M. Veiga Rodrigues, C. Sievers, J.W. Medlin, Enhanced hydrothermal stability of γ-Al_2O_3 catalyst supports with alkyl phosphonate coatings, Langmuir 34 (12) (2018) 3619–3625, https://doi.org/10.1021/acs.langmuir.8b00465.
[71] A.W. Scaroni, R.G. Jenkins, P.L. Walker Jr., Coke deposition on Co-Mo/Al_2O_3 and Co-Mo/C catalysts, Appl. Catal. 14 (1985) 173–183, https://doi.org/10.1016/S0166-9834(00)84353-5.
[72] H. Kobayashi, H. Yokoyama, B. Feng, A. Fukuoka, Dehydration of sorbitol to isosorbide over H-beta zeolites with high Si/Al ratios, Green Chem. 17 (5) (2015) 2732–2735, https://doi.org/10.1039/C5GC00319A.